Journal of Power Sources 269 (2014) 520–525

Contents lists available at ScienceDirect

Journal of Power Sources

journal homepage: www.elsevier.com/locate/jpowsour

Plasma enhanced chemical vapor deposition silicon nitride for a high-performance lithium ion battery anode

Jinho Yang [a], Rhet C. de Guzman [b], Steven O. Salley [b], K.Y. Simon Ng [b], Bing-Hung Chen [c], Mark Ming-Cheng Cheng [a, *]

[a] Department of Electrical and Computer Engineering, Wayne State University, Detroit, MI 48202, United States
[b] Department of Chemical Engineering and Materials Science, Wayne State University, Detroit, MI 48202, United States
[c] Department of Chemical Engineering, National Cheng-Kung University, Tainan, Taiwan

HIGHLIGHTS

- Silicon nitride was evaluated as a lithium ion battery anode.
- PECVD was adapted to tune chemical composition for high performance silicon anodes.
- Silicon nitride has a high reversible capacity and stable cyclability.
- The capacity remained 76% over 100 cycles for thick films (~1 μm).
- High capacity retention was contributed to a Li_3N conductive matrix and good adhesion.

ARTICLE INFO

Article history:
Received 25 April 2014
Received in revised form
21 June 2014
Accepted 24 June 2014
Available online 10 July 2014

Keywords:
Lithium ion battery
Silicon anode
Silicon nitride
Composite anode

ABSTRACT

Silicon nitride thin films deposited by plasma enhanced chemical vapor deposition (PECVD) were evaluated for their performance as lithium ion battery anodes. PECVD is a mature technique in the semiconductor industry, but has been less utilized in battery research. We show that PECVD is a powerful tool to control the chemical composition of battery materials and its corresponding specific capacity. A 250 nm nitride anode was shown to have a stable reversible capacity of 1800 mAh g^{-1} with 86% capacity retention after 300 cycles. The capacity dropped for thicker films (1 μm), where it retained 76% after 100 cycles. The high reversible capacity of the PECVD nitride anode was attributable to a conductive Li_3N matrix and excellent adhesion between PECVD films and copper current collectors.

1. Introduction

Silicon has a theoretical specific capacity of 3579 mAh g^{-1} (which corresponds to $Li_{15}Si_4$ formation) for lithium ion battery anodes [1,2]. The major drawback for the silicon anode, however, is poor cyclability due to the large volume expansion (>300%) associated with Si–Li alloy formation during charge and discharge. The mechanical stress induced by the volume change causes material degradation and loss of electrical contact, which results in rapid capacity fading. In recent years, silicon nanostructures and composites have been investigated to overcome mechanical degradation and to permit a good cyclic life [3,4]. Incorporation of other materials in silicon potentially can limit the volume expansion, such as copper (inactive material) [5,6], carbon (active material) [7,8], oxygen [3,9,10], and nitrogen [11,12]. Among these materials, nitride has been less investigated ($Si_{0.76}N_{0.24}$, $SiN_{0.92}$) [11,12]. Silicon nitride has been shown to be converted into silicon with the formation of lithium nitride (Li_3N) by the reaction in Equation (1) [12]. The reaction potential of the conversion reaction of nitride has been shown to be below 1 V vs Li.

$$SiN_x + yLi^+ + ye^- \rightarrow Si + xLi_{y/x}N \quad (1)$$

The resultant silicon can react with lithium in a further reduction while the ductile and conductive Li_3N matrix buffers volume expansion of the Si–Li alloy in Equation (2). The control of silicon and nitride composition is critical because stoichiometric silicon nitride ($SiN_{1.33}$) behaves like an electrical insulator, which leads to extremely low charge and discharge capacity.

* Corresponding author. Tel.: +1 313 577 5462.
E-mail address: mcheng@wayne.edu (M.M.-C. Cheng).

http://dx.doi.org/10.1016/j.jpowsour.2014.06.135
0378-7753/

$$Si + xLi^+ + xe^- \leftrightarrow Li_xSi \quad (2)$$

Plasma enhanced chemical vapor deposition (PECVD) is a process to deposit films by ionizing reactive gases with plasma at low temperature (100–350 °C). PECVD is a versatile manufacturing process. Amorphous silicon (*a*-Si) with varied chemical composition (e.g., doped with oxygen, nitrogen, fluorine etc.) can be fabricated [13]. PECVD has been widely used in the microelectronics and photovoltaic industries. The advantages of PECVD are a high deposition rate, a rapid process and a conformal coating for three-dimensional nanostructures [14] compared to other processes such as low pressure CVD [15,16], physical vapor deposition (PVD) [9,10,17,18] and atomic layer deposition (ALD). Although the PECVD method has been used for silicon-based anodes in several papers [19–22], the rapid capacity fading was observed in those experiments.

In this work, PECVD silicon nitride films were evaluated as lithium ion battery anodes. Nitrogen (N_2) instead of ammonia (NH_3) was utilized as the nitrogen sources during deposition. The chemical composition and nanostructure of PECVD films were tuned by different deposition parameters (power and temperature), and their electrochemical performance was evaluated including reversible capacity, Coulombic efficiency, and cyclability. The amorphous and elastic PECVD silicon nanostructures coupled with a nitride matrix may accommodate the volumetric variation during charge and discharge processes without severe mechanical pulverization.

2. Experimental

Preparation of copper substrates: 25 μm thick copper foil was purchased from Lyon Industries Inc. The copper foil was first chemically etched by 0.1 M ferric chloride ($FeCl_3$) for 5 min. After etching, the copper foil was rinsed with DI water and isopropyl alcohol (IPA). The sample was dried on a heater at 70 °C for 5 min.

Deposition of amorphous silicon (*a*-Si) and silicon nitride: *a*-Si and silicon nitride films were deposited on as-prepared copper foils using PECVD (Plasma Therm 790). The deposition parameters for *a*-Si were 100% SiH_4, flow rate 5 sccm, temperature 100 °C, pressure 450 mTorr and radio frequency (RF) power 25 W. Nitride was deposited by diluted silane (2% SiH_4 in 98% N_2). The typical deposition parameters for nitride were flow rate 50 sccm, temperature 350 °C, pressure

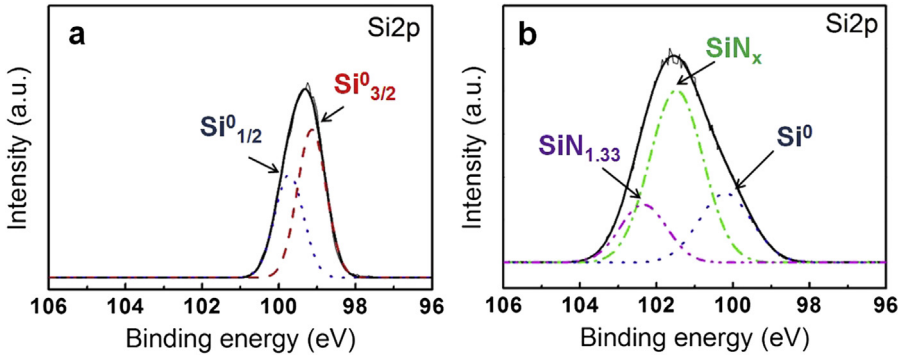

Fig. 1. The high resolution XPS spectra of Si 2p of (a) PECVD *a*-Si and (b) PECVD nitride.

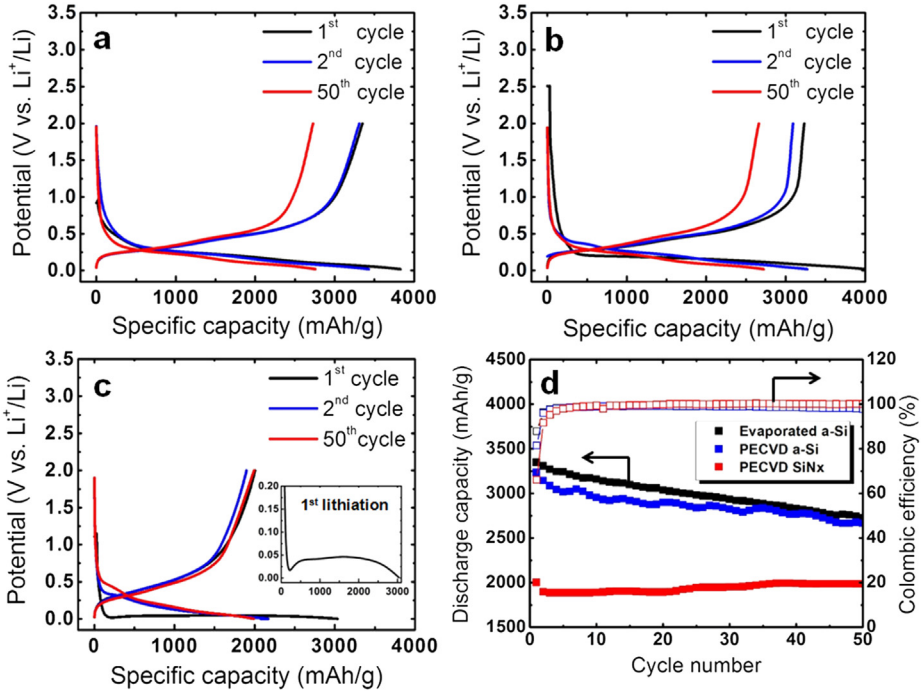

Fig. 2. The voltage profiles during 50 cycles for (a) evaporated *a*-Si and (b) PECVD *a*-Si, and (c) PECVD nitride. (d) The cycling performance of three samples.

450 mTorr and RF power 25 W. Films deposited at different temperature (100 °C, 200 °C, 300 °C) and RF power (25 W, 50 W, 100 W) were also evaluated. The thickness of films was measured using a surface profiler (Dektak 8). Electron beam evaporated *a*-Si (using Temescal BJD 1800) was also deposited as a control. The weights of the *a*-Si and nitride films were measured by a microbalance (Mettler Toledo, XP26) before and after thin film deposition. The balance had the accuracy of 1 μg. Prior to the film deposition, the copper foils were dried in a vacuum oven in order to remove moisture.

Electrochemical tests: The electrochemical characteristics of the *a*-Si and nitride films were measured by a half-cell configuration. All the cell assembly and electrochemical testing were performed in a glove box filled with ambient Argon. The cell was assembled using a CR2032 coin cell. Lithium metal (Alfa Aesar) was used as counter and reference electrodes. A polyethylene separator (Celgard 2320) was soaked overnight in the liquid electrolyte (1 mol $LiPF_6$ in ethylene carbonate (EC) and dimethyl carbonate (DMC) with a 1:1 ratio). The charge and discharge tests were performed using a potentiostat (Maccor Model 4200) at a constant current density of 2 A g^{-1}. The cut-off voltages were set 0.001 V and 2 V versus Li^+/Li.

Characterizations: X-ray photoelectron spectroscopy (XPS) was used to analyze chemical composition of *a*-Si and nitride with a PHI 5500 ESCA (Perkin Elmer). The x-ray power was 210 W, and the emission current was 15 mA. Neutralization was performed to prevent charging effects. A survey (0–1200 eV) and high-resolution analysis on each element with 23.5 eV pass energy were performed. After electrochemical tests, the cells were disassembled and then rinsed with DMC solvent. Scanning electron microscopy (SEM, JEOL JSM-6510LV) was used to image surface morphologies of samples before and after cycling. The acceleration voltage was 15 kV in SEM. High-resolution transmission electron microscopy (TEM, Titan) was conducted to image the surface of nitride films with its high resolution (300 kV) after 300 cycles. A thin sample of anode was prepared with a dual-beam focus ion beam (FIB, TESCAN LYRA).

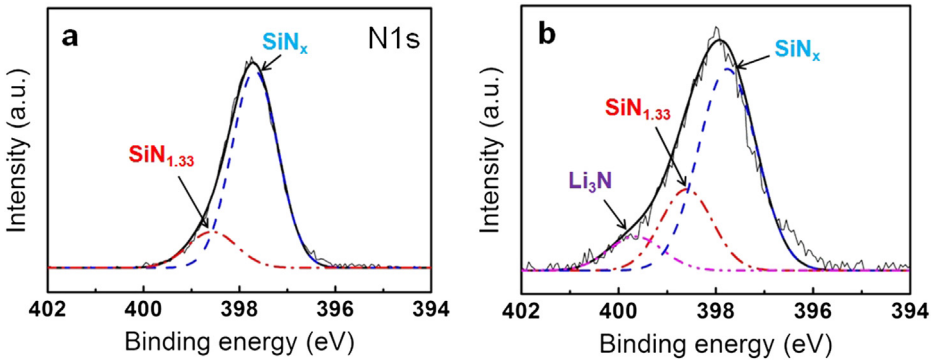

Fig. 3. The high resolution N 1s spectra of the Si-rich nitride anode (a) before cycle, and (b) after 100 cycles.

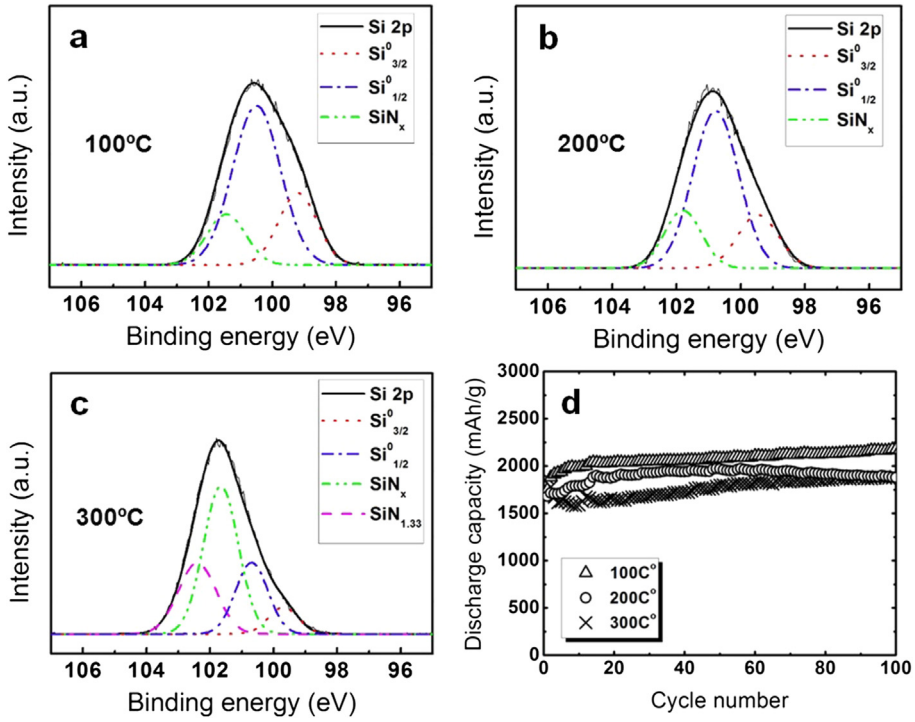

Fig. 4. The high resolution XPS spectra of the Si 2p for PECVD nitride deposited (a) at 100 °C, (b) 200 °C, and (c) 300 °C. (d) The cycling performance of three samples grown at different temperatures.

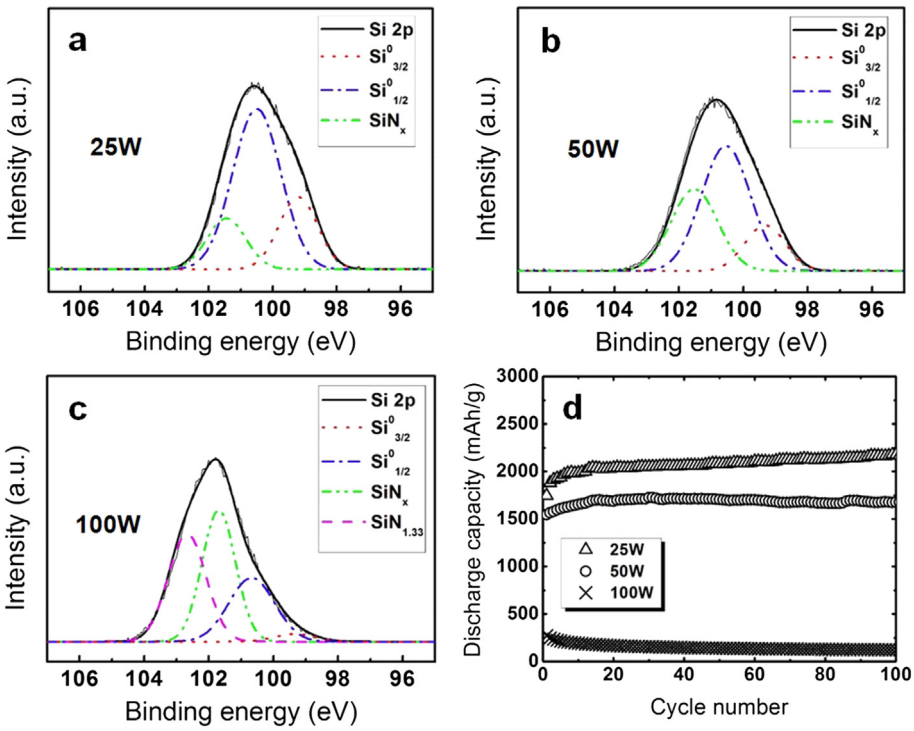

Fig. 5. The high resolution XPS spectra of the Si 2p for PECVD nitride deposited (a) at 25 W, (b) 50 W, and (c) 100 W. (d) The cycling performance of three samples grown at different plasma RF powers.

3. Results and discussion

Fig. 1 shows the XPS Si 2p spectra of PECVD *a*-Si and nitride before cycling. The *a*-Si film was composed of Si^0. Compared to *a*-Si, the Si 2p spectrum of nitride consisted of a broad peak. In Fig. 1b, the Si 2p spectrum was fitted using three Gaussian functions of Si^0 (100.07 eV), SiN_x (101.48 eV), and $SiN_{1.33}$ (102.34 eV). The ratios of $SiN_{1.33}$, SiN_x and Si^0 were determined to be 13%, 70%, and 17%, respectively. In Fig. 3a, the N 1s spectrum of nitride was fitted using two Gaussian functions of $SiN_{1.33}$ (398.65 eV) and SiN_x (397.71 eV). The ratio of $SiN_{1.33}$ and SiN_x was determined to be 16% and 84%, respectively. Using XPS survey, the atomic concentration of silicon and nitrogen in nitride was 57% and 43%, respectively. Based on the fitting, the value x in SiN_x was estimated to be 0.83.

Fig. 2 illustrates the charge and discharge curves of evaporated *a*-Si, PECVD *a*-Si and PECVD nitride. These films were cycled at 1C, which referred to 1-h charge. Fig. 2a and b shows the charge and discharge curves of first, second and 50th cycles of *a*-Si deposited by evaporation and PECVD, respectively. In this study, cathodic lithiation in the anode was referred to charge. In the first charge, the voltage plateaus for the evaporated and PECVD *a*-Si films were slightly different (0.3 V and 0.24 V respectively). The voltage plateau corresponds to the formation of Si–Li alloys. The first charge capacity for evaporated and PECVD *a*-Si films were similar (3827 and 3993 mAh g^{-1} respectively). The value was slightly higher than the theoretical specific capacity (3579 mAh g^{-1}) probably associated with the accuracy of weight measurements. The following discharge curve had a voltage plateau around 0.37 V for both evaporated and PECVD *a*-Si films. The first discharge capacity for evaporated and PECVD *a*-Si were 3348 mAh g^{-1} and 3233 mAh g^{-1}, making Coulombic efficiency 87% and 81%, respectively. The initial capacity loss was probably due to electrolyte reduction reactions, resulting in solid-electrolyte interphase (SEI) formation [23,24]. The Coulombic efficiency for the samples became approximately 99.2% after a couple of cycles, but dropped to 97.8% afterwards. The capacity retention of evaporated *a*-Si was slightly higher than that of PECVD *a*-Si.

In Fig 2c, PECVD nitride showed a different voltage profile compared to *a*-Si films. At the initial stage of the first charge, the voltage profile had a potential overshoot, which indicated the nucleation of a new phase to form Li_3N during the conversion reaction [25]. The first discharge capacity of PECVD nitride was 2004 mAh g^{-1}, corresponding to a 66% Coulombic efficiency. The low Coulombic efficiency could be attributed to irreversible conversion reaction in addition to SEI formation. The Coulombic efficiency increased during the second and third cycle and maintained almost 100% for the rest of cycles. The discharge capacity at the 50th cycle was 1984 mAh g^{-1}. PECVD nitride had a higher capacity retention (99%) compared to PECVD *a*-Si (84%). The incorporation of nitrogen limited the specific capacity but improved the cycling stability.

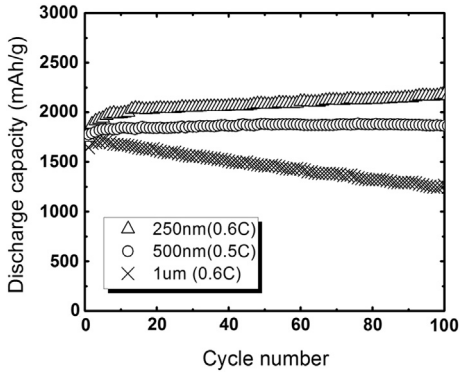

Fig. 6. The cycling performances of 250 nm, 500 nm, and 1 μm PECVD nitride anodes during 100 cycles. All three films were deposited at 25 W power and 100 °C.

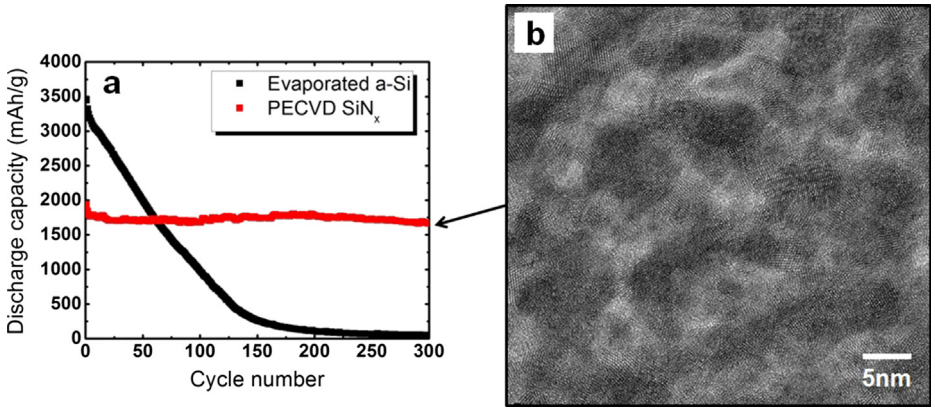

Fig. 7. (a) The cycling performances of 250 nm thick evaporated *a*-Si and PECVD nitride during 300 cycles. (b) A TEM image of PECVD nitride after 300 cycles.

The Li–N matrix after cycling was studied using XPS. Fig. 3 shows the high resolution N 1s spectra of the nitride before and after 100 cycles. Before reactions, the spectrum (Fig. 3a) of N1s was fitted by two Gaussian functions SiN_x and $SiN_{1.33}$, and their ratio was 84% and 16%, respectively. After 100 cycles, the spectrum (Fig. 3b) was fitted by three Gaussian functions. The ratio of SiN_x and $SiN_{1.33}$ became 66% and 24%, indicating that SiN_x was oxidized to nonconductive $SiN_{1.33}$ during multiple cycles. In addition, a new peak was present at 399.7 eV, which was ascribed to Li_3N. Li_3N has high ionic conductivity ($2–5 \times 10^{-4}$ S cm^{-1}), which may play a role in facilitating Li ion transport [26,27].

The deposition parameters (such as temperature and power) for PECVD nitride have been studied in order to tune chemical compositions and its electrochemical properties. The common nitrogen source in PECVD nitride is ammonia (NH_3), and it produces hydrogen rich nitride [28,29]. Using N_2 instead of NH_3 as the nitrogen source, a low hydrogen content silicon nitride is obtained. N_2 has an inherently higher binding energy than NH_3, which hinders ionization. With higher temperature and higher power during deposition, N_2 could dissociate into free nitrogen active species. Fig. 4 shows the high resolution XPS spectra of the Si 2p and corresponding cycling performance of PECVD nitride deposited at different temperatures (100 °C, 200 °C, and 300 °C) with a constant RF power of 25 W. The concentration of nitrogen increased with increasing deposition temperature (Fig. 4a–c). PECVD nitride deposited at lower temperature (100 °C) had slightly higher specific capacity. Fig. 5 shows the high resolution XPS spectra of the Si 2p and cycling performance of PECVD nitride deposited at RF power of 25 W, 50 W, and 100 W at a constant temperature 100 °C. The atomic ratio of silicon to nitrogen decreased with increasing RF power. In addition, silicon became more oxidized with the increasing RF power. The specific capacity of nitride was very sensitive to RF power during deposition, and it decreased with increasing RF power. In Fig. 5d, nitride deposited at 100 W was shown to have an extremely low specific capacity. The highly oxidized silicon and nonconductive $SiN_{1.33}$ caused deteriorated effects on the cyclic performance.

The increase in film thickness is desired for practical uses in batteries. Fig. 6 shows the cycling performance of 250 nm, 500 nm, and 1 μm PECVD nitride anodes deposited at 100 °C and 25 W RF power. The discharge capacity at the 100th cycle was 2100, 1880, and 1450 mAh g^{-1}, respectively. The samples were tested at 0.6 C. The 250 nm and 500 nm samples showed high capacity retention (~100%) upon 100 cycles compared to 1 μm nitrides (76%). Thick films showed a lower discharge capacity due to higher electrical resistance (and ohmic drop) [30,31]. Thick films also showed a poor cycling performance that was associated with the stress induced material degradation.

250 nm evaporated *a*-Si and PECVD nitride anodes were tested for 300 cycles and the results are shown in Fig. 7a. In the initial 50 cycles, the capacity of evaporated *a*-Si was higher than the PECVD nitride. Nevertheless, the capacity of evaporated *a*-Si gradually dropped during cycling. PECVD nitride showed a stable cyclic performance. Under inspection by SEM, large cracks were found in evaporated *a*-Si and silicon eventually peeled-off from the substrate. On the other hand, PECVD nitride formed small islands (diameter 5–7 μm) and well adhered to the substrate (Figure S1). The adhesion of evaporated silicon and PECVD nitride were investigated using a scotch tape test (Figure S2). Compared to evaporated silicon, PECVD nitride showed a very good adhesion probably due to ion bombardment of reactive gases during the deposition. Fig. 7b shows a high resolution TEM image of PECVD nitride after 300 cycles. The lattice structure of silicon nanocrystal (diameter of 5–10 nm) was clearly seen. The silicon nanocrystals were uniformly embedded in a matrix made of Li_3N and electrolyte decomposition. Li_3N acts as a barrier to prevent the aggregation of silicon nanocrystals and maintained structural stability [32]. In addition, Li_3N is known to have a high ionic conductivity, which may enhance the charge transfer during lithiation and delithiation. Compared to other conversion anode material such as silicon oxide, nitride has been found to have a higher Coulombic efficiency over a large number of cycles [3].

4. Conclusion

We adapted a PECVD process using SiH_4 and N_2 to deposit silicon nitride for a lithium ion battery anode. PECVD nitride deposited at low RF power exhibited a higher reversible capacity than bare *a*-Si. The incorporation of nitrogen reduced the specific capacity of the anode but dramatically improved the cyclic stability. Silicon nitride was converted into silicon with the formation of Li_3N by a conversion reaction. TEM of nitride after 300 cycles confirms that silicon nanocrystals were uniformly embedded in a conductive Li_3N matrix which prevented aggregation of the Si nanoparticles, resulting in stable cyclability. In the future, we anticipate nitride can be made into powders for lithium ion battery industry.

Acknowledgements

The authors would like to thank Dan Durisin and Bill Funk for their assistances using nFab facility, Chris Thrush for the access of XPS, Li Li for AFM imaging, and TESCAN Inc for the access of FIB and

TEM. The financial supports from WSU, NSF (#1229635), DOE and Richard Barber Foundation are gratefully acknowledged.

Appendix A. Supplementary data

Supplementary data related to this article can be found at http://dx.doi.org/10.1016/j.jpowsour.2014.06.135.

References

[1] M.N. Obrovac, L. Christensen, Electrochem. Solid State Lett. 7 (2004) A93–A96.
[2] M.N. Obrovac, L.J. Krause, J. Electrochem. Soc. 154 (2007) A103–A108.
[3] J. Yang, Y. Takeda, N. Imanishi, C. Capiglia, J.Y. Xie, O. Yamamoto, Solid State Ionics 152 (2002) 125–129.
[4] J.R. Szczech, S. Jin, Energy Environ. Sci. 4 (2011) 56–72.
[5] J.P. Maranchi, A.F. Hepp, A.G. Evans, N.T. Nuhfer, P.N. Kumta, J. Electrochem. Soc. 153 (2006) A1246–A1253.
[6] P. Limthongkul, Y.I. Jang, N.J. Dudney, Y.M. Chiang, J. Power Sources 119 (2003) 604–609.
[7] A.M. Wilson, J.R. Dahn, J. Electrochem. Soc. 142 (1995) 326–332.
[8] K. Hanai, Y. Liu, N. Imanishi, A. Hirano, M. Matsumura, T. Ichikawa, Y. Takeda, J. Power Sources 146 (2005) 156–160.
[9] M. Miyachi, H. Yamamoto, H. Kawai, T. Ohta, M. Shirakata, J. Electrochem. Soc. 152 (2005) A2089–A2091.
[10] H. Takezawa, K. Iwamoto, S. Ito, H. Yoshizawa, J. Power Sources 244 (2013) 149–157.
[11] D. Ahn, C. Kim, J.G. Lee, B. Park, J. Solid State Chem. 181 (2008) 2139–2142.
[12] N. Suzuki, R.B. Cervera, T. Ohnishi, K. Takada, J. Power Sources 231 (2013) 186–189.
[13] M.I. Alayo, I. Pereyra, W.L. Scopel, M.C.A. Fantini, Thin Solid Films 402 (2002) 154–161.
[14] R.W. Collins, A.S. Ferlauto, G.M. Ferreira, C. Chen, J. Koh, R.J. Koval, Y. Lee, J.M. Pearce, C.R. Wronski, Sol. Energy Mater. Sol. Cells 78 (2003) 143–180.
[15] S. Bourderau, T. Brousse, D.M. Schleich, J. Power Sources 81 (1999) 233–236.
[16] H.J. Jung, M. Park, Y.G. Yoon, G.B. Kim, S.K. Joo, J. Power Sources 115 (2003) 346–351.
[17] T. Takamura, S. Ohara, M. Uehara, J. Suzuki, K. Sekine, J. Power Sources 129 (2004) 96–100.
[18] V. Baranchugov, E. Markevich, E. Pollak, G. Salitra, D. Aurbach, Electrochem. Commun. 9 (2007) 796–800.
[19] T.L. Kulova, A.M. Skundin, Y.V. Pleskov, E.I. Terukov, O.I. Kon'kov, J. Electroanal. Chem. 600 (2007) 217–225.
[20] J.J. Nguyen, K. Evanoff, W.J. Ready, Thin Solid Films 519 (2011) 4144–4147.
[21] M.W. Forney, R.A. DiLeo, A. Raisanen, M.J. Ganter, J.W. Staub, R.E. Rogers, R.D. Ridgley, B.J. Landi, J. Power Sources 228 (2013) 270–280.
[22] S.O. Kim, H.T. Shim, J.K. Lee, J. Solid State Electrochem. 14 (2010) 1247–1253.
[23] M. Winter, J.O. Besenhard, M.E. Spahr, P. Novak, Adv. Mater. 10 (1998) 725–763.
[24] T.D. Hatchard, J.R. Dahn, J. Electrochem. Soc. 151 (2004) A838–A842.
[25] A. Netz, R.A. Huggins, W. Weppner, J. Power Sources 119 (2003) 95–100.
[26] U.V. Alpen, A. Rabenau, G.H. Talat, Appl. Phys. Lett. 30 (1977) 621–623.
[27] W. Li, G.T. Wu, C.M. Araujo, R.H. Scheicher, A. Blomqvist, R. Ahuja, Z.T. Xiong, Y.P. Feng, P. Chen, Energy Environ. Sci. 3 (2010) 1524–1530.
[28] J.H. Souk, G.N. Parsons, J. Batey, Amorph. Silicon Technol. 219 (1991) 787–792.
[29] L. Wang, H.S. Reehal, F.L. Martinez, E.S. Andres, A. del Prado, Semicond. Sci. Technol. 18 (2003) 633–641.
[30] M. Yoshio, T. Tsumura, N. Dimov, J. Power Sources 146 (2005) 10–14.
[31] S.W. Song, K.A. Striebel, R.P. Reade, G.A. Roberts, E.J. Cairns, J. Electrochem. Soc. 150 (2003) A121–A127.
[32] J. Cho, J. Mater. Chem. 20 (2010) 4009–4014.